Journal of Physics D: Applied Physics

PAPER

Single β-Ga_2O_3 microbelt solar-blind photodetector with high specific detectivity, high rejection ratio and fast speed

To cite this article: Zhiyao Zheng *et al* 2022 *J. Phys. D: Appl. Phys.* **55** 365107

View the article online for updates and enhancements.

You may also like

- Review of polymorphous Ga_2O_3 materials and their solar-blind photodetector applications
Xiaohu Hou, Yanni Zou, Mengfan Ding et al.
- Review of deep ultraviolet photodetector based on gallium oxide
Yuan Qin, , Shibing Long et al.
- Methods for synthesizing -Ga_2O_3 thin films beyond epitaxy
Jacqueline Cooke, Berardi Sensale-Rodriguez and Leila Ghadbeigi

This content was downloaded from IP address 159.226.165.22 on 02/03/2023 at 01:26

IOP Publishing Journal of Physics D: Applied Physics
J. Phys. D: Appl. Phys. **55** (2022) 365107 (8pp) https://doi.org/10.1088/1361-6463/ac77c9

Single β-Ga_2O_3 microbelt solar-blind photodetector with high specific detectivity, high rejection ratio and fast speed

Zhiyao Zheng[1,2], Kewei Liu[1,2,*], Zhen Cheng[1], Baoshi Qiao[1], Xing Chen[1], Chang Zhou[1,2], Jialin Yang[1], Qiu Ai[1], Yongxue Zhu[1], Binghui Li[1], Lei Liu[1,2] and Dezhen Shen[1,2,*]

[1] State Key Laboratory of Luminescence and Applications, Changchun Institute of Optics, Fine Mechanics and Physics, Chinese Academy of Sciences, No. 3888 Dongnanhu Road, Changchun 130033, People's Republic of China
[2] Center of Materials Science and Optoelectronics Engineering, University of the Chinese Academy of Sciences, Beijing 100049, People's Republic of China

E-mail: liukw@ciomp.ac.cn and shendz@ciomp.ac.cn

Received 5 April 2022, revised 24 May 2022
Accepted for publication 10 June 2022
Published 30 June 2022

Abstract

An ideal solar-blind photodetector should possess high responsivity, low dark current, high speed, high spectral selectivity, high stability and a facile fabrication method. In this work, a high-quality single β-Ga_2O_3 microbelt photodetector is fabricated through low-pressure chemical vapor deposition and *in situ* atmospheric pressure annealing techniques. Due to the high quality and low defect density, this device shows a peak responsivity of 9.47 A W^{-1} at 256 nm, a dark current of 1 pA and an ultrashort fall time of 1.37 μs under 20 V bias. Moreover, an ultrahigh specific detectivity of $\sim 10^{14}$ Jones and an extremely large solar-blind/ultraviolet A rejection ratio of nearly 10^5 have also been achieved, suggesting the excellent sensitivity and wavelength selectivity of our single β-Ga_2O_3 microbelt photodetector. Besides that, the β-Ga_2O_3 microbelt photodetector exhibits excellent mechanical and long-term stabilities. Our findings provide a facile and promising route to develop high performance solar-blind UV photodetectors.

Keywords: β-Ga_2O_3 microbelt, solar-blind photodetector, high quality, high performance

(Some figures may appear in colour only in the online journal)

1. Introduction

Since the solar radiation at 200–280 nm (solar-blind ultraviolet) is strongly absorbed by ozone in the atmosphere and cannot reach the earth's surface, the photodetectors working in this waveband, widely known as solar-blind photodetectors, have the advantages of low background interference and high sensitivity, which have been widely used in military and civil fields [1–7]. An ideal solar-blind UV detector should have high responsivity, high spectral selectivity, low dark current and high response speed [8]. Compared with conventional photomultiplier tubes and Si-based ultraviolet photodetectors, solar-blind ultraviolet photodetectors based on wide-band gap semiconductors (Ga_2O_3, AlGaN, $ZnGa_2O_4$, ZnMgO, diamond, etc) offer special superiorities such as all solid state, low

* Authors to whom any correspondence should be addressed.

 © 2022 IOP Publishing Ltd

power consumption and no filter required, which have become a current research hotspot [9–19]. Among these wide band-gap semiconductors, Ga_2O_3-related materials, especially β-Ga_2O_3 have attracted the increasing attention due to their intrinsic solar-blind band gap (4.7–5.1 eV), high radiation hardness and excellent thermal and chemical stability [20, 21]. To date, various device geometries including metal-semiconductor-metal (MSM) photodetectors, heterojunction/Schottky barrier photodiodes, and phototransistors have been demonstrated on Ga_2O_3 bulk, thin films or nanostructures [22–26]. Surprisingly, high responsivity (>1 A W^{-1}) has been widely achieved in different types of Ga_2O_3-based photodetectors [27–29]. Nevertheless, present Ga_2O_3 solar-blind photodetectors commonly suffered from slow response speed, large dark current, and low solar-blind/UV rejection ratio, which may be related to high sub-band-gap response, strong trapping effect, and high donor concentration caused by low crystalline quality and extensive oxygen vacancies of Ga_2O_3. Although homoepitaxy and high temperature oxygen annealing have been commonly used to improve the crystal quality and reduce the oxygen vacancy density, they still cannot meet the needs of high-speed, low dark current and high rejection ratio UV detection [30–32].

Compared to bulk and thin film counterparts, the materials that naturally grown into one-dimensional (1D) nano/microstructures are more likely to achieve high crystalline perfection and reduced defects [33–35]. Moreover, 1D nano/microstructured semiconductors also have the advantages of large specific surface area, light weight, good flexibility, and low cost. Therefore, solar-blind UV detectors based on 1D β-Ga_2O_3 have recently emerged as one of the most promising approaches to improve the photodetection performance [29, 36–46]. In particular, β-Ga_2O_3 nano/microbelts (sheets or ribbons) photodetectors have been highlighted for their high responsivity ($\sim10^2$–$\sim10^4$ A W^{-1}) [29, 34, 37, 47, 48]. However, the reported solar-blind photodetectors based on 1D β-Ga_2O_3 nano/microbelts commonly suffer from the low solar-blind/UVA (ultraviolet A) rejection ratio ($\sim10^2$–$\sim10^4$) and slow response speed ($\sim$0.1 few seconds), which should be associated with surface defects and polycrystalline formation [41, 45, 49]. As a result, the performance of solar-blind UV detectors based on 1D β-Ga_2O_3 is still lower than expected.

In this paper, high-quality single-crystal β-Ga_2O_3 microbelts are grown by low-pressure chemical vapor deposition (CVD) and *in-situ* atmospheric pressure annealing technologies. The β-Ga_2O_3 microbelts show high crystalline quality, few oxygen vacancies and very flat surface. The MSM structure solar-blind UV detector is fabricated on an individual β-Ga_2O_3 microbelt with 100 μm channel length. The fabricated device shows a low dark current of 10^{-12} A, a peak responsivity of 9.47 A W^{-1} at 256 nm and a fast decay time of 1.37 μs. Moreover, the device has almost no response to 365 nm illumination with a highest solar-blind/UVA rejection ratio ($R_{peak}/R_{365\ nm}$) of nearly 10^5. In addition, the device could keep high performance under bending state.

2. Experimental details

One-dimensional β-Ga_2O_3 microbelts were grown via a low-pressure CVD and *in-situ* atmospheric pressure annealing technologies. To prepare Ga_2O_3 microbelts, Ga_2O_3 and graphite (C) high-purity powers (99.99%) with a weight ratio of 1:1 served as the precursor mixtures. Ga_2O_3/graphite mixed powder and oxygen gas were used as Ga and O sources, respectively. The mixed powder was placed in a corundum boat and then slowly pushed into a tube furnace. After that, the tube furnace was pumped down to a base vacuum using a mechanical pump and heated up to 900 °C at a speed of 15 °C min^{-1}. At this point (900 °C), the mechanical pump was turned off. Subsequently, Ar and O_2 gases with a flow ratio of 6:1 were introduced into the tube, so that the pressure in the tube reached $\sim$0.05 MPa. Then the temperature was slowly increased at 3 °C min^{-1}, and at the same time, β-Ga_2O_3 microbelts began to grow. And the following reactions might take place in the tube furnace:

$$\mathrm{C\,(s) + Ga_2O_3\,(s) \rightarrow Ga\,(g) + CO_2\,(g)} \tag{1}$$

$$\mathrm{Ga\,(g) + O_2\,(g) \rightarrow Ga_2O_3\,(s)\,.} \tag{2}$$

After 60 min, the temperature was raised to 1080 °C, and the growth of the microbelts was completed. Subsequently, Ar and O_2 gases were continuously introduced into the tube and the pressure inside the tube was increased and maintained at atmospheric pressure. Then the microbelts were annealed *in-situ* at 1080 °C in Ar and O_2 atmospheres for 60 min at the atmospheric pressure to improve the crystalline quality and repair oxygen vacancy defects. Finally, the tube furnace was slowly cooled down to room temperature, and the high-quality β-Ga_2O_3 microbelts can be obtained at the edge of corundum boat (figure 1(a)). The MSM photodetector was fabricated on an individual β-Ga_2O_3 microbelt by sputtering 30 nm thick gold electrodes using a shadow mask on a flexible substrate, and the distance between two electrodes is 100 μm.

The characterizations of the Ga_2O_3 microbelts were investigated by scanning electron microscopy (SEM, HITACHI S-4800), transmission electron microscopy (TEM, FEI Talos F200s), x-ray diffraction (XRD, Bruker D8GADDS) with Cu Kα radiation (λ = 0.154 nm), x-ray photoelectron spectroscopy (XPS) spectrometer (Thermo ESCALAB 250) and Raman spectrometer (Finder Vista) with a 532 nm laser. Current–voltage (*I–V*) and time–dependent current (*I–t*) curves of the photodetector were obtained using a semiconductor device analyzer (Agilent B1500A). The photoresponse spectrum was measured through responsivity measurement system equipped with an SR 830 lock-in amplifier and a 150 W Xe lamp. The transient responses were recorded by a Tektronics DPO5104 oscilloscope under 260 nm laser excitation with a pulse width of 10 ns.

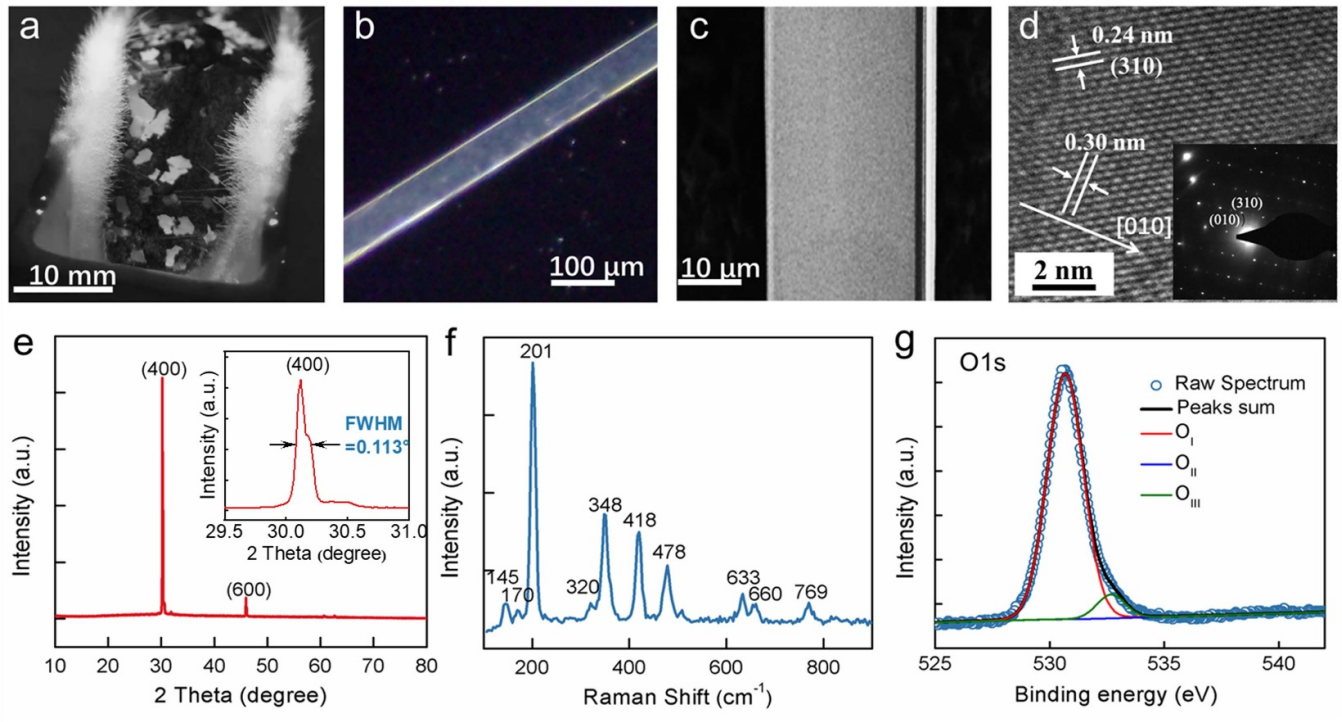

Figure 1. (a) Photograph, (b) optical micrograph, (c) SEM images, (d) high-resolution TEM (HRTEM) and selected area electron diffraction (SAED) images, (e) XRD pattern, (f) Raman spectroscopy and (g) O1s XPS spectrum of the β-Ga_2O_3 microbelt.

3. Results and discussion

Figures 1(a)–(c) show the photograph, the optical micrograph and the SEM image of the as-prepared materials, indicating that these products are available in microbelt shapes with typical widths of 5–120 μm, thicknesses of 0.1–2 μm and lengths of 1–12 mm. Clearly, the surface of the microbelts is very flat and smooth. Figure 1(d) shows a high-resolution TEM (HRTEM) image taken from the edge of the thin Ga_2O_3 microbelt. The distances between adjacent layers are about 0.30 and 0.24 nm, corresponding to (010) and (310) planes of β-Ga_2O_3 with a monoclinic structure, respectively. The corresponding selected area electron diffraction (SAED) image of Ga_2O_3 microbelt is shown in the inset of figure 1(d). Figure 1(e) presents the XRD pattern of multiple β-Ga_2O_3 microbelts laid flat on a sample stage. Two strong diffraction peaks at $2\theta = 30.1°$ and 45.9° correspond to the (400) and (600) crystal faces of monoclinic β-Ga_2O_3, respectively (JCPDS card No. 43-1012), and the peak positions are in agreement with the reported values of the single-crystal bulk β-Ga_2O_3 [25, 50, 51]. The inset of figure 1(e) shows a magnified (400) diffraction peak of β-Ga_2O_3 microbelts and its full-width half maximum is estimated to be ~0.113°. No extra peaks can be observed in the XRD spectrum. HRTEM, SAED and XRD results suggest that the length and thickness directions of these Ga_2O_3 microbelts are along the [010] and [100] orientations, respectively. To further analyze the structural property of β-Ga_2O_3 microbelts, Raman spectroscopy was performed on a single microbelt at room temperature as shown in figure 1(f). According to the previous reports, the peaks located below 200 cm^{-1} reflect to low-frequency vibration and translation of tetrahedra–octahedra chains. The peaks at 300–500 cm^{-1} are associated with the deformation of tetrahedra and the translation of octahedra. The peaks at 600–800 cm^{-1} are ascribed with the stretching and bending of tetrahedra [52–54]. Notably, the Raman peak positions of our β-Ga_2O_3 microbelts are in good agreement with those for the previously reported bulk β-Ga_2O_3, suggesting the low defect density in β-Ga_2O_3 microbelts [52, 55, 56]. Figure 1(g) presents the high-resolution XPS O1s spectrum of β-Ga_2O_3 microbelts, which can be deconvoluted into two peaks centered at 530.68 eV (O_I) and 532.682 eV (O_{III}). The peak at 530.68 eV can be assigned to the lattice oxygen in the β-Ga_2O_3 and the peak at 532.682 eV is generally considered to be the specific chemisorbed oxygen [57, 58]. Notably, the absence of the oxygen vacancy-related peak located near 531 eV (O_{II}) indicates that our β-Ga_2O_3 microbelts have extremely low oxygen vacancy defect density.

Figure 2(a) shows the *I*–*V* characteristic curves of the device in dark and under different illumination conditions. Under 20 V bias, the dark current of the device is only 1 pA, which is lower than that of the most reported Ga_2O_3 photodetectors [38, 39, 59–61]. Upon 254 nm illumination (650 μW cm^{-2}), the current shows a significant increase and the photo to dark current ratio can reach five orders of magnitude at 20 V. More interestingly, the device has an ultra-weak response to 365 nm illumination (1050 μW cm^{-2}), suggesting an excellent UVA rejection. The *I*–*V* curves of the device under 365 and 254 nm illumination show a huge difference, which can be understood as follows: when the 254 nm

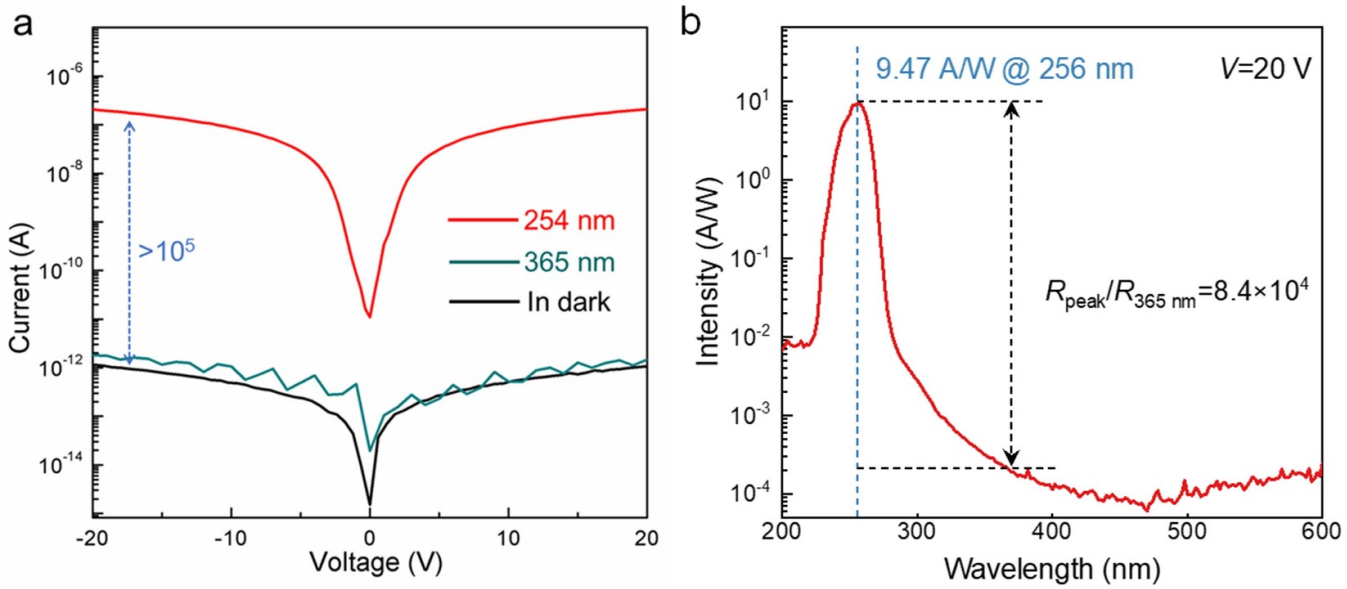

Figure 2. (a) *I–V* curves in dark and under 365 and 254 nm illuminations. (b) The spectral response property of the β-Ga_2O_3 solar-blind UV detector at a bias voltage of 20 V.

UV light is irradiated on the device, Ga_2O_3 absorbs light with photon energy greater than the semiconductor band gap, producing a large number of photo-generated carriers (electron–hole pairs). As a result, the resistivity of Ga_2O_3 is reduced significantly. The photo-generated electrons and holes can be separated under the electric field, and then collected by the electrodes, which leads to the generation of large photocurrent. In contrast, when the 365 nm UV light is irradiated on the device, most photons pass through Ga_2O_3, and sub-bandgap defect-related absorption is very weak due to the high crystalline quality and few oxygen vacancy defects. Therefore, the device shows almost the same *I–V* curves both in dark and under 365 nm illumination. The photoresponse spectrum of the individual β-Ga_2O_3 microbelt photodetector is shown in figure 2(b). The device shows a peak responsivity of 9.47 A W^{-1} at 256 nm with -3 dB cutoff wavelength of 264 nm, which is in good agreement with the bandgap of β-Ga_2O_3. More interestingly, the solar-blind/UV rejection ratio ($R_{\text{peak}}/R_{365\text{ nm}}$) can reach as high as 8×10^4. In addition, the specific detectivity (D^*) is a critical parameter to describe the smallest detectable signal, which can be estimated by [62]

$$D^* = (S\Delta f)^{\frac{1}{2}}/\text{NEP} \tag{3}$$

where S is the effective illuminated area of the device, Δf is the bandwidth, and noise equivalent power (NEP) can be estimated by

$$\text{NEP} = I_n/R \tag{4}$$

where R is the responsivity, I_n is the noise current. For MSM solar-blind photodetectors, the noise is usually dominated by dark current shot noise, and thus I_n can be simply expressed as $(2qI_d\Delta f)^{\frac{1}{2}}$, where q is the electronic charge and I_d is the dark current. So that, the D^* can be obtained by a more general equation [63–65]:

$$D^* = R/(2qI_d/S)^{\frac{1}{2}}. \tag{5}$$

The D^* value of the device at the wavelength of 256 nm was calculated to be as high as 1.67×10^{14} Jones at the bias of 20 V due to the high responsivity and low dark current.

Figure 3(a) shows the *I–t* curves of the device with different applied voltages under 254 nm illumination at a fixed power density of 650 μW cm^{-2}. With increasing the voltage, the quick and stable on/off switching behavior can be well maintained. Meanwhile, the photocurrent increases linearly with the increase of bias voltage due to the enhanced drift velocity of the carriers (the inset). The time–dependent photoresponse measurement was carried out under different optical power densities at 20 V as shown in figure 3(b). And the photocurrent as a function of power density taken from the *I–t* curves was shown in the inset of figure 3(b). The nice linear relationship between photocurrent and optical power density can be clearly obtained, which is a strong and direct evidence of the high crystalline quality and low defect density of β-Ga_2O_3 microbelt, indicating the potential application of our device in light measurement and imaging [22, 66].

The response speed is another important figure of merit for UV photodetectors. To accurately obtain the response time of the device, the transient response was recorded using a 260 nm pulsed laser (10 ns pulse width and 10 Hz) and a digital oscilloscope as shown in figure 4. The 90%–10% fall time is only $\sim$1.37 μs and the current can rapidly return to its initial dark-state value within 50 μs after the laser pulse.

To meet the requirements of practical applications, the mechanical and long-term stabilities of β-Ga_2O_3 microbelt solar-blind photodetector have been investigated. By bending the substrate at different angles, the mechanical stress can be

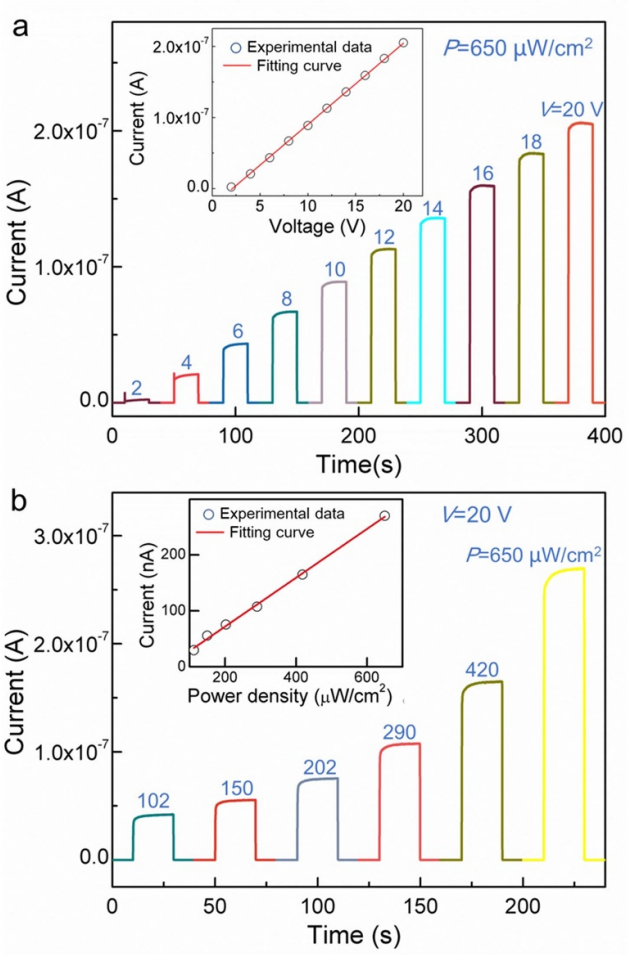

Figure 3. (a) *I–t* curves at different applied bias voltages under 254 nm light illumination with the intensity of 650 μW cm^{-2}, and the inset is the photocurrent as a function of voltage. (b) *I–t* curves under 254 nm illumination with different intensities biased at 20 V, and the inset is the photocurrent as a function of illumination intensity.

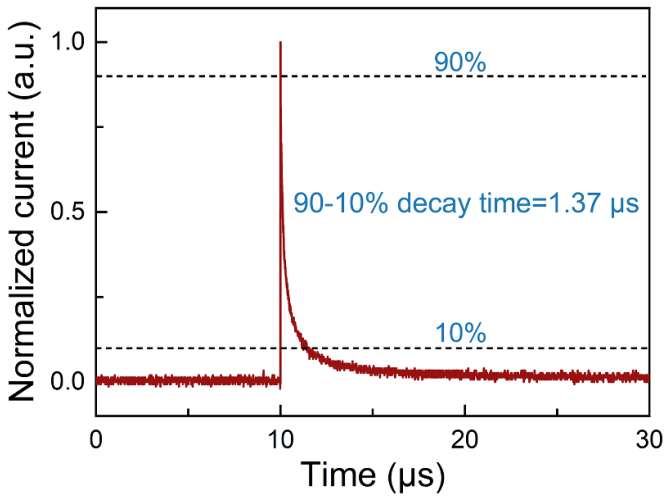

Figure 4. The transient response of the device under 260 nm pulsed laser at 20 V.

introduced in the microbelt as shown in the inset of figure 5(a). At 20 V bias, the device exhibits almost constant performance under different bending states, suggesting an excellent mechanical stability (figure 5(a)). Moreover, the photoresponse behavior of β-Ga_2O_3 microbelt solar-blind photodetector remains unchanged after storing it under ambient environment for at least 3 months as presented in figure 5(b). This result indicates that the β-Ga_2O_3 microbelt-based photodetector possesses good long-term stability.

The excellent device performance in this work can be attributed to the high crystalline quality and few oxygen vacancies of the β-Ga_2O_3 microbelt, which is mainly realized by the following points: (a) compared with atmospheric pressure CVD, low pressure CVD provides a larger free diffusion distance of reactant gas molecules, a slower growth rate and higher purity, which is beneficial to obtain high crystalline quality β-Ga_2O_3 microbelts. (b) *In-situ* high-temperature post-annealing in Ar and O_2 atmospheres can further improve the crystalline quality of the β-Ga_2O_3 microbelts and help to repair oxygen vacancy defects. Table 1 summarizes the comparison of the performance parameters of the recently reported 1D β-Ga_2O_3-based solar-blind UV photodetectors. Obviously, our single β-Ga_2O_3 microbelts solar-blind UV detector in this work has an ultrafast response speed with a decay time of only 1.37 μs, which is more than three orders of magnitude faster than that of the previously reported 1D Ga_2O_3

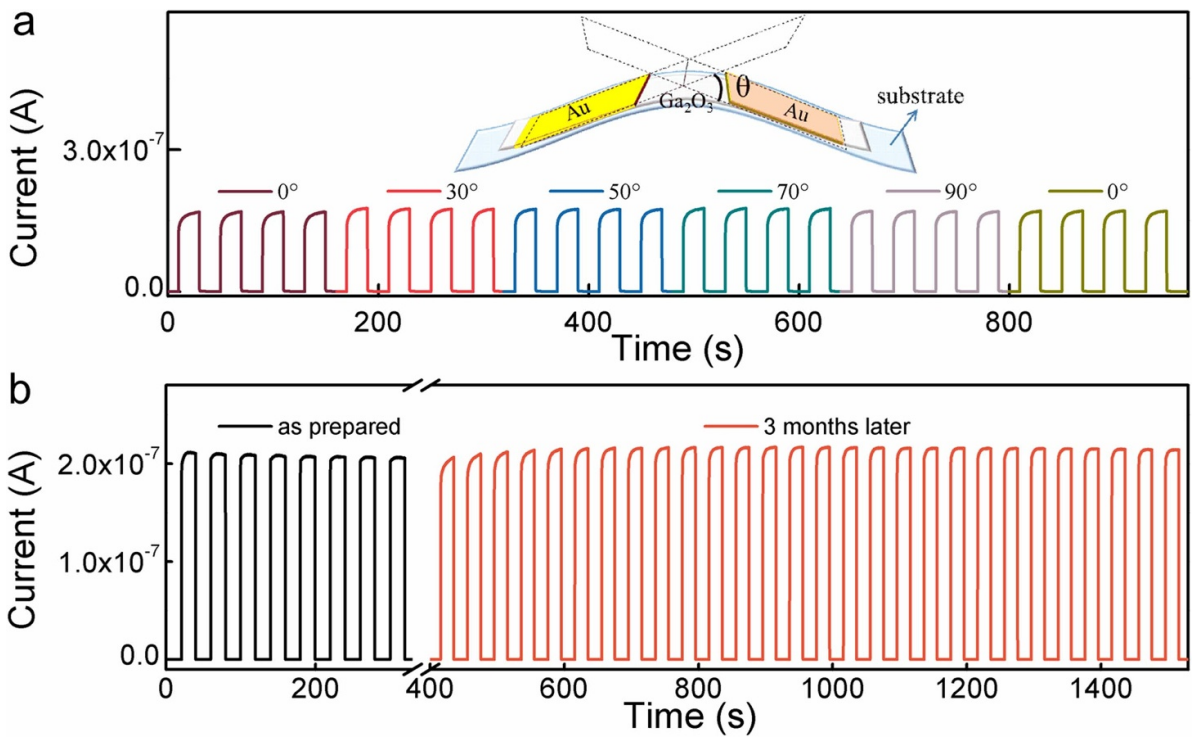

Figure 5. Time–dependent photoresponse curves of the device (a) under different bending conditions and (b) after storage in air for 3 months.

Table 1. Performance comparison of representative 1D β-Ga_2O_3 based solar-blind UV detectors.

Materials	Structure	Bias (V)	Dark current (A)	Responsivity (A W^{-1})	Solar-blind/UV rejection ratio	Decay time (s)	D^* (Jones)	References
Ga_2O_3 nanobelt	MSM	30	—	$\sim 10^2$	—	<0.3	—	[29]
In-doped Ga_2O_3 nanobelt	MSM	6	1×10^{-13}	547	—	<0.6	—	[34]
Ga_2O_3 multi-nanobelt	MSM	20	1×10^{-13}	851	—	<0.3	—	[37]
Ga_2O_3/PANI	p–n	0	—	2.1×10^{-2}	—	8.14×10^{-3}	1.5×10^{11}	[40]
Ga_2O_3 micro/nano-sheet	Schottky	1	$\sim 10^{-10}$	19.31	—	0.023	—	[38]
β-Ga_2O_3 nanowires	MSM	6	3.25×10^{-10}	0.128	46.28 ($R_{254\ nm}/R_{365\ nm}$)	3.188	3.676×10^{10}	[41]
β-Ga_2O_3 nanowires	MSM	5		0.122	—	0.012	—	[39]
β-Ga_2O_3/GaN nanowires	Heterojunction	10	1.6×10^{-10}	2.75×10^{-2}	—	0.23	1.2×10^{11}	[42]
β-Ga_2O_3 nanowires	MSM	10	7.73×10^{-10}	233	—	0.04	8.16×10^{12}	[43]
β-Ga_2O_3 nanowires	MSM	20	8×10^{-9}	0.71	—	0.19	—	[44]
Ga_2O_3/GaN nanowire array	Vertical heterojunction	5	—	753.2	—	<0.04	—	[36]
β-Ga_2O_3 nanowires	MSM	10	8×10^{-12}	—	$\sim 10^3$ ($R_{231\ nm}/R_{290\ nm}$)	<0.5	—	[45]
Ga_2O_3	MSM	20	1×10^{-12}	9.47	8×10^4 ($R_{254\ nm}/R_{365\ nm}$)	1.37×10^{-6}	1.67×10^{14}	This work

devices. Moreover, owing to the ultralow dark current and relatively high responsivity, our device exhibits the highest specific detectivity of $\sim 10^{14}$ Jones and the highest solar-blind/UV rejection ratio of nearly 10^5, among the photodetectors based on Ga_2O_3 1D structures reported so far. The devices with high solar blind/UV rejection ratio and high-speed have important application prospects in practical applications high frequency and weak signal detection.

4. Conclusions

In this work, the high-quality β-Ga_2O_3 microbelts were prepared through low-pressure CVD and *in-situ* atmospheric pressure annealing technologies. Solar-blind UV detector with MSM structure was fabricated using a single β-Ga_2O_3 microbelt with two gold electrodes spaced 100 μm apart. The device exhibits a low dark current of $\sim 10^{-12}$ A, a peak responsivity of 9.47 A W^{-1} at 256 nm and an ultrashort decay time of 1.37 μs at the bias of 20 V. Moreover, the specific detectivity of $\sim 10^{14}$ Jones and solar-blind/UVA rejection ratio ($R_{peak}/R_{365\ nm}$) of nearly 10^5 have also been achieved in this work, which are much higher than those of the previously reported Ga_2O_3 1D micro/nanostructure photodetectors. Besides that, β-Ga_2O_3 microbelt photodetector exhibits excellent mechanical and long-term stabilities. Our findings provide a feasible method to develop high performance, high stable and flexible solar-blind UV photodetectors.

Data availability statement

All data that support the findings of this study are included within the article (and any supplementary files).

Acknowledgments

This work is supported by the National Natural Science Foundation of China (Nos. 62074148, 61875194, 11727902, 12074372, 11774341, 11974344, 61975204, and 11804335), the National Ten Thousand Talent Program for Young Top-notch Talents, the Key Research and Development Program of Changchun City (No. 21ZY05), the 100 Talents Program of the Chinese Academy of Sciences, Youth Innovation Promotion Association, CAS (No. 2020225), Jilin Province Science Fund (20210101145JC).

Author contributions

The manuscript was written through contributions of all authors. Zhiyao Zheng: Investigation, Writing-original draft. Kewei Liu: Validation, Formal analysis, Writing-review and editing, Supervision, Resources. Zhen Cheng, Resources, Visualization. Baoshi Qiao, TEM analyse. Xing Chen, Resources, Visualization. Chang Zhou, Investigation. Jialin Yang: Supervision. Qiu Ai, Supervision. Yongxue Zhu, Supervision. Binghui Li: Resources, Supervision. Lei Liu: Resources, Supervision. Dezhen Shen: Writing-review and editing, Supervision, Resources. All authors have given approval to the final version of the manuscript.

Conflict of interest

There are no conflicts to declare.

ORCID iDs

Kewei Liu https://orcid.org/0000-0001-9778-4996
Baoshi Qiao https://orcid.org/0000-0002-5095-1344
Binghui Li https://orcid.org/0000-0002-6704-2809
Lei Liu https://orcid.org/0000-0002-9714-2130

References

[1] Chang M *et al* 2022 *J. Phys. D: Appl. Phys.* **55** 035103
[2] Liu Z, Zhang S, Zhi Y, Li S, Yan Z, Chu X, Bian A, Li P and Tang W 2021 *J. Phys. D: Appl. Phys.* **54** 195104
[3] Varshney U, Aggarwal N and Gupta G 2022 *J. Mater. Chem.* C **10** 1573
[4] Li S *et al* 2021 *J. Phys. Chem. Lett.* **12** 447
[5] Xie C, Lu X, Liang Y, Chen H, Wang L, Wu C, Wu D, Yang W and Luo L 2021 *J. Mater. Sci. Technol.* **72** 189
[6] Xie C, Lu X-T, Tong X-W, Zhang Z-X, Liang F-X, Liang L, Luo L-B and Wu Y-C 2019 *Adv. Funct. Mater.* **29** 1806006
[7] Xie C and Yan F 2017 *Small* **13** 1701822
[8] Li S *et al* 2019 *ACS Appl. Mater. Interfaces* **11** 35105
[9] Li Y, Xiu X, Xu W, Zhang L, Xie Z, Tao T, Chen P, Liu B, Zhang R and Zheng Y 2021 *J. Phys. D: Appl. Phys.* **54** 014003
[10] Ma Y *et al* 2021 *J. Phys. D: Appl. Phys.* **54** 305101
[11] Cai Q, You H, Guo H, Wang J, Liu B, Xie Z, Chen D, Lu H, Zheng Y and Zhang R 2021 *Light Sci. Appl.* **10** 94
[12] Chen Y, Zhou X, Zhang Z, Miao G, Jiang H, Li Z and Song H 2021 *Mater. Lett.* **291** 129583
[13] Han D, Liu K, Chen X, Li B, Zhai T, Liu L and Shen D 2021 *Appl. Phys. Lett.* **118** 251101
[14] Wang Z, Lin J, Wei X, Zheng W and Hu Q 2021 *Front. Mater.* **8** 787613
[15] Chen X, Wang L, Liu K, Zhang Z, Li B, Wu J, Wang J, Ni Y and Shen D 2020 *J. Mater. Chem.* C **8** 1089
[16] Tsai S H, Basu S, Huang C Y, Hsu L C, Lin Y G and Horng R H 2018 *Sci. Rep.* **8** 14056
[17] Han D, Liu K, Hou Q, Chen X, Yang J, Li B, Zhang Z, Liu L and Shen D 2020 *Sens. Actuators* A **315** 112354
[18] Liu Z, Ao J-P, Li F, Wang W, Wang J, Zhang J and Wang H-X 2016 *Appl. Phys. Lett.* **109** 153507
[19] Liang Y, Ma M, Zhong X, Xie C, Tong X, Xing K and Wu C 2021 *IEEE Electron Device Lett.* **42** 1192
[20] Ma Y J *et al* 2022 *Vacuum* **198** 110886
[21] Tang X *et al* 2022 *ACS Appl. Mater. Interfaces* **14** 1304
[22] Tak B R, Kumar S, Kapoor A K, Wang D, Li X, Sun H and Singh R 2021 *J. Phys. D: Appl. Phys.* **54** 453002
[23] Zheng Y, Hasan M N and Seo J H 2021 *Adv. Mater. Technol.* **6** 2100254
[24] Qiao B, Zhang Z, Xie X, Li B, Li K, Chen X, Zhao H, Liu K, Liu L and Shen D 2019 *J. Phys. Chem.* C **123** 18516
[25] Feng Q *et al* 2016 *IEEE Trans. Electron Devices* **63** 3578
[26] Khan M, Kadam V, Sant T, Jejurikar S M, Joshi K, Bhopale S R, More M A and Late D 2020 *Mater. Chem. Phys.* **254** 123512
[27] Wang Y H *et al* 2021 *ACS Nano* **15** 16654
[28] Pratiyush A S, Krishnamoorthy S, Solanke S V, Xia Z, Muralidharan R, Rajan S and Nath D N 2017 *Appl. Phys. Lett.* **110** 221107
[29] Li L, Auer E, Liao M, Fang X, Zhai T, Gautam U K, Lugstein A, Koide Y, Bando Y and Golberg D 2011 *Nanoscale* **3** 1120
[30] Chen M, Zhang Z, Lv Z, Zhan R, Chen H, Jiang H and Chen J 2022 *ACS Appl. Nano Mater.* **5** 351
[31] Li Z M *et al* 2020 *Vacuum* **178** 109448

[32] Nishinaka H, Nagaoka T, Kajita Y and Yoshimoto M 2021 *Mater. Sci. Semicond. Proc.* **128** 105732
[33] Lian Q *et al* 2019 *Small* **15** 1900236
[34] Tian W, Zhi C, Zhai T, Chen S, Wang X, Liao M, Golberg D and Bando Y 2012 *J. Mater. Chem.* **22** 17984
[35] Li S X, Xu Y S, Li C L, Guo Q, Wang G, Xia H, Fang H H, Shen L and Sun H B 2020 *Adv. Mater.* **32** 2001998
[36] He T *et al* 2019 *Adv. Opt. Mater.* **7** 1801563
[37] Zou R, Zhang Z, Liu Q, Hu J, Sang L, Liao M and Zhang W 2014 *Small* **10** 1848
[38] Oh S, Mastro M A, Tadjer M J and Kim J 2017 *ECS J. Solid State Sci.* **6** Q79
[39] Zhang L *et al* 2020 *Nanophotonics* **9** 4497
[40] Wang Y, Li L, Wang H, Su L, Chen H, Bian W, Ma J, Li B, Liu Z and Shen A 2020 *Nanoscale* **12** 1406
[41] Zhang M, Kang S, Wang L, Zhang K, Wu Y, Feng S and Lu W 2021 *J. Phys. D: Appl. Phys.* **54** 175106
[42] Ding W and Meng X 2021 *J. Alloys Compd.* **866** 157564
[43] Xie C, Lu X T, Ma M R, Tong X W, Zhang Z X, Wang L, Wu C Y, Yang W H and Luo L B 2019 *Adv. Opt. Mater.* **7** 1901257
[44] Wang S *et al* 2019 *J. Alloys Compd.* **787** 133
[45] Du J, Xing J, Ge C, Liu H, Liu P, Hao H, Dong J, Zheng Z and Gao H 2016 *J. Phys. D: Appl. Phys.* **49** 425105
[46] Zhang Z G, Wang X X, Zhang J, Yu M, Zhang J C, Zhang H D and Long Y Z 2018 *J. Alloys Compd.* **752** 359
[47] Oh S, Kim J, Ren F, Pearton S J and Kim J 2016 *J. Mater. Chem.* C **4** 9245
[48] Kim J, Oh S, Kim S and Kim J 2019 Ga_2O_3 nanobelt devices *Gallium Oxide* (Amsterdam: Elsevier) p 331
[49] Ohira S, Sugawara T, Nakajima K and Shishido T 2005 *J. Alloys Compd.* **402** 204
[50] Xiang H C, Han S, Lu Y M, Cao P J, Liu W J, Zeng Y X, Jia F, Xu W Y, Liu X K and Zhu D L 2018 *J. Alloys Compd.* **747** 869
[51] Wang D, He L, Le Y, Feng X, Luan C, Xiao H and Ma J 2020 *Ceram. Int.* **46** 4568
[52] Dohy D, Lucazeau G and Revcolevschi A 1982 *J. Solid State Chem.* **45** 180
[53] Onuma T, Fujioka S, Yamaguchi T, Itoh Y, Higashiwaki M, Sasaki K, Masui T and Honda T 2014 *J. Cryst. Growth* **401** 330
[54] Kumar S, Dhara S, Agarwal R and Singh R 2016 *J. Alloys Compd.* **683** 143
[55] Zhao Y and Frost R L 2008 *J. Raman Spectrosc.* **39** 1494
[56] Kranert C, Sturm C, Schmidt-Grund R and Grundmann M 2016 *Sci. Rep.* **6** 35964
[57] Liu S, Jiao S, Lu H, Nie Y, Gao S, Wang D, Wang J and Zhao L 2022 *J. Alloys Compd.* **890** 161827
[58] Weng T F, Ho M S, Sivakumar C, Balraj B and Chung P F 2020 *Appl. Surf. Sci.* **533** 147476
[59] Cao J, Chen L, Chen X, Zhu Y, Dong J, Wang B, He M and Wang X 2021 *Crystals* **11** 1248
[60] Tan P *et al* 2021 *Adv. Opt. Mater.* **9** 2100173
[61] Zhong M, Wei Z, Meng X, Wu F and Li J 2015 *J. Alloys Compd.* **619** 572
[62] Fang Y, Armin A, Meredith P and Huang J 2018 *Nat. Photon.* **13** 1
[63] Kim S and Kim J 2020 *Appl. Phys. Lett.* **117** 261101
[64] Wang Y *et al* 2019 *Appl. Phys. Lett.* **114** 011103
[65] Oh S, Kim C-K and Kim J 2017 *ACS Photonics* **5** 1123
[66] Zheng Z, Liu K, Chen X, Qiao B, Ma H, Liu D, Liu L and Shen D 2021 *Nanotechnology* **32** 475201